A simultaneous dual-polarity mass spectrometer with electron start for MeV-SIMS

Author(s):
Miltenberger, Klaus-Ulrich; Döbeli, Max; Vockenhuber, Christof; Synal, Hans-Arno

Publication date:
2021-11-15

Permanent link:
https://doi.org/https://doi.org/10.3929/ethz-b-000510175

Originally published in:
Nuclear Instruments and Methods in Physics Research Section B: Beam Interactions with Materials and Atoms 507, https://doi.org/10.1016/j.nimb.2021.09.010

Funding acknowledgement:
- New Developments in Ion Beam Physics ()

Nuclear Instruments and Methods in Physics Research B 507 (2021) 36–41

Contents lists available at ScienceDirect

Nuclear Inst. and Methods in Physics Research, B

journal homepage: www.elsevier.com/locate/nimb

A simultaneous dual-polarity mass spectrometer with electron start for MeV-SIMS

Klaus-Ulrich Miltenberger *, Max Döbeli, Christof Vockenhuber, Hans-Arno Synal

Laboratory of Ion Beam Physics, ETH Zürich, Otto-Stern-Weg 5, CH-8093 Zürich, Switzerland

ARTICLE INFO

Keywords:
MeV-SIMS
ToF-SIMS
Dual-polarity SIMS
Cluster ions
Secondary ion yield

ABSTRACT

The Capillary Heavy Ion MeV-SIMS Probe (CHIMP) at ETH Zürich has been redesigned with a second mass spectrometer and symmetric extraction to enable simultaneous analysis of positive and negative secondary ions. Secondary electrons are deflected within the negative spectrometer and detected independently. The fast secondary electron signal is used as a start signal for both Time-of-Flight mass spectrometers.

The new setup enables the simultaneous acquisition and analysis of both secondary ion polarities emitted under identical conditions from the same sample location. This allows to study correlations between secondary ions of different polarities emitted from a single primary ion impact. Measurements with small primary C_n cluster ions show the influence of cluster size on the multiplicity of secondary ion emission. Furthermore, a cluster effect in the ratio between positive and negative ion yields of corresponding secondary ion species is identified, with the ratio approaching parity for larger cluster sizes n.

1. Introduction

MeV-SIMS (Secondary Ion Mass Spectrometry) achieves high yields of large molecular secondary ions by bombarding a sample surface with primary ions in the MeV energy range. This has been demonstrated in several studies so far [1,2] and is generally attributed to the enormous electronic stopping power of the primary ions in this energy regime prevailing over their much smaller nuclear stopping power. However, the underlying desorption and ionization processes are not well understood yet.

The predominant mechanism occurring with primary beam energies in the MeV range is electronic sputtering, where most of the energy of the incident particles is deposited into the electronic subsystem of the sample material. Finally, the removal of an atom or molecule can be facilitated by a range of different processes to transfer energy to the particle and break its bonds. More in-depth overviews of the proposed theoretical models were compiled [3,4] but the theoretical approaches mostly focus on the desorption effect and largely neglect the ionization process.

Most experimental setups detect and measure charged secondary particles of only one polarity at a time. Thus, it is especially difficult to separate the processes of secondary particle desorption and ionization of the desorbed particles. To eliminate the influence of ionization processes post-ionization of the secondary particles with a laser [5] has been used. However even in this case difficulties to quantify the actually reached post-ionization efficiency make it difficult to directly compare the measurements with those of secondary ions acquired without post-ionization [6]. Another possibility to get a more differentiated picture of the secondary ionization mechanisms involved is to compare positive and negative secondary ion spectra acquired from the sample under identical conditions. Such an approach would ultimately require the simultaneous measurement of positive and negative secondary ions. A first setup implementing a suitable dual-polarity ToF (Time-of-Flight) mass spectrometer has been developed for simultaneous mass analysis of secondary ion spectra in MALDI (matrix-assisted laser desorption/ionization) [7]. More recently, a system has been developed for integration into a commercial (conventional) keV-SIMS instrument [8]. In order to apply this approach for the characterization of secondary ion desorption in MeV-SIMS, the existing CHIMP (Capillary Heavy Ion MeV-SIMS Probe) instrument at ETH Zürich was rebuilt into a Dual-ToF spectrometer. The new instrument features two symmetrically arranged linear ToF mass spectrometers for the simultaneous detection of both positive and negative secondary ions. Additionally, a magnetic separation and an independent detection of secondary electrons inside the negative arm of the ToF spectrometer has been implemented. This enables the use of the secondary electrons to generate a fast start signal for

* Corresponding author.
E-mail address: mklaus@phys.ethz.ch (K.-U. Miltenberger).

https://doi.org/10.1016/j.nimb.2021.09.010
Received 22 June 2021; Received in revised form 14 September 2021; Accepted 15 September 2021
Available online 4 October 2021

both secondary ion ToF spectrometers.

In the following the construction and functional principles of the novel dual-polarity ToF system are described and the results of a first set of measurements are presented and discussed.

2. Experimental setup

The initial setup of the CHIMP measurement chamber has been described in two earlier publications [9,10]: The MeV-SIMS chamber is installed behind the high energy electrostatic analyser (acting as an E/q filter) of the AMS (Accelerator Mass Spectrometry) beamline of the ETH Zurich 6 MV Tandem accelerator facility [11]. Consequently, the beam path exclusively contains electrostatic ion optical elements except for the low energy mass analyser at the ion source ($m\ E/q^2 < 15000$ u keV/e^2) which limits the maximum ion mass to about 750 u at 17 keV injection energy. This enables the use of monoatomic primary ion beams with energies of up to 80 MeV and of molecular or cluster primary ion beams with up to 15 MeV. The energy of the cluster primary ion beams is limited in this setup due to the maximum E/q ratio achievable using the HE-ESA in charge state 2+ (without dissociation of the cluster).

A schematic view of the upgraded Dual-ToF spectrometer setup inside the modified CHIMP chamber is given in Fig. 1. In front of the MeV-SIMS measurement chamber, the primary ion beam passes through two sets of adjustable collimation slits. Inside the chamber it is then collimated to micrometer diameters by either a tapered glass capillary [12] or a set of micrometer apertures mounted on a two axis piezo driven goniometer and rotator stage. This allows the adjustment of the collimation system to the incident beam direction by maximizing the count rate in a gas ionization chamber (GIC) [13] mounted in transmission geometry. This detector is also used for the measurement of the primary ion count rate with the sample moved out of the way before and after each yield measurement.

Samples are mounted on a piezo driven xy-stage with the primary beam incident along the surface normal. A sample magazine with five samples can be loaded into the measurement chamber via a vacuum lock, from which individual samples are then transferred onto the sample stage using a mechanical feedthrough.

Positive and negative secondary ions as well as secondary electrons are extracted under an angle of 45° with respect to the sample surface normal in a mirror-symmetrical extraction geometry into a positive (pToF) respectively negative (nToF) Time-of-flight spectrometer. The extraction stage of both mass spectrometers was redesigned to allow for a more efficient extraction of secondary particles and to create the same extraction field geometry for secondary particles of both polarities. In contrast to more common single-polarity ToF extraction settings, a heavily biased extraction or even an extraction potential applied to the sample was not an option. This would severely compromise the extraction efficiency and mass resolution of at least one of the mass spectrometers. A photograph of the sample region of the CHIMP chamber is provided in Fig. 2.

Both mass spectrometers feature a two-stage extraction coupled with an einzel lens and electrostatic steerer plates, respectively. Within the negative ToF spectrometer, the secondary electrons are separated from the secondary ions. They are deflected onto a separate electron detector by means of a weak external magnetic field. Although such a separation is already achieved based on the earth magnetic field, it can be increased and optimized by either the positioning of permanent magnets on the outside of the nToF spectrometer flange or by a concentric coil (tilted 15° with respect to the ion flight path). The electron detector consists of a dual annular MCP stack in Chevron configuration (two MCPs type PS34099, 50 mm outside diameter and 15 mm centre hole diameter, Photonis Scientific Inc., Sturbridge, MA, USA) integrated into the nToF flight tube. At the end of both the pToF and nToF mass spectrometers, stop detectors are mounted. They consist of a dual MCP stack in Chevron configuration each (two MCPs type F1094-01, Hamamatsu Photonics K. K., Hamamatsu, Japan). The signal from the negatively biased detector (positive ion MCP) is directly available on ground potential from the anode. The signals from both positively biased detectors (negative ion MCP, electron MCP) are coupled out from the high voltage and transferred to ground potential via high voltage capacitors.

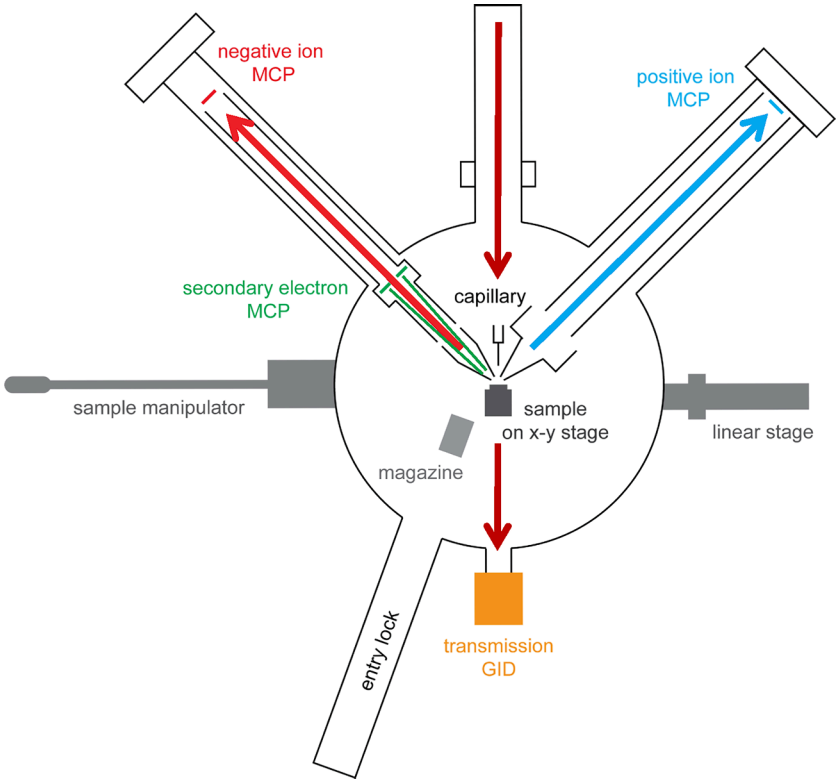

Fig. 1. Schematic view of the MeV-SIMS chamber with the dual-polarity symmetric extraction mass spectrometers.

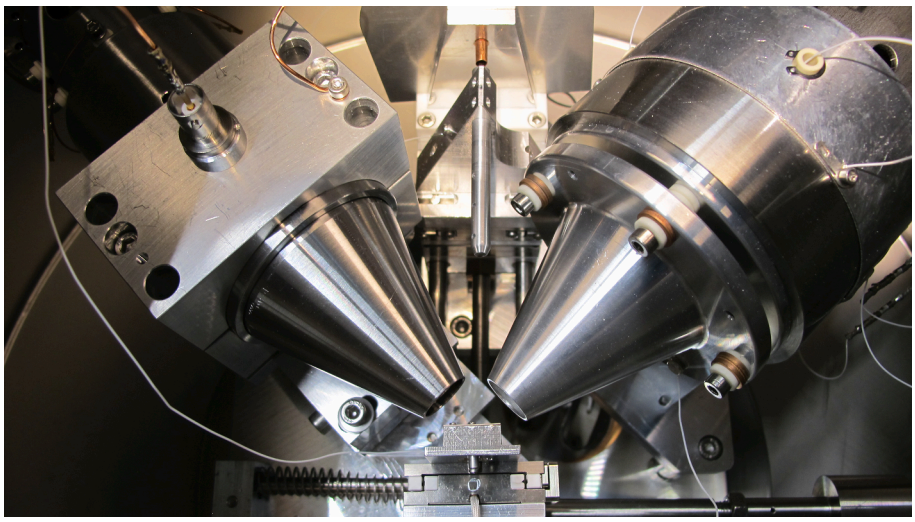

Fig. 2. Picture of the measurement setup with beam collimation apertures (primary beam entering from the top) between the nToF (left) and pToF (right) extraction cones. The empty piezo sample stage is visible at the bottom of the picture.

The electron and secondary ion detector signals are amplified and fed into constant fraction discriminators. The discriminator output signals are read into separate channels of a 1 GHz CAEN DT5751 digitizer and stored into sequential event files with a timing resolution of 1 ns. The fourth digitizer channel can be used to simultaneously record timing signals from the optional beam pulsing or GIC detector. Online analysis of the data is used to provide a live preview of the acquired ToF spectra within the LabView data acquisition software. The event-based recording allows for later offline analysis. Therefore, the data can be analysed using various different coincidence conditions between secondary electron, beam pulsing, transmitted primary ion and secondary ion signals. Worth of particular mention is that this does not put any restriction on maximum flight time or the number of stop signals that can be correlated with an individual start signal. This enables the study of correlated particle emission from a single projectile impact.

Upon impact of a primary ion onto the sample surface, the fast secondary electrons emitted are detected first and provide the start signal for the flight time measurements of the slower positive and negative secondary ions. For each secondary electron signal detected (acting as the ToF start signal) all possible stop signals falling within a certain coincidence time window (usually 20 μs, corresponding to a mass range up to approx. 650u) are considered and the resulting flight times are calculated and collected in a histogram to obtain a ToF spectrum. In a second analysis step the obtained ToF spectra are mass calibrated based on distinct mass peaks identified from reference spectra of known sample materials.

The primary design goal was to achieve the simultaneous detection of positive and negative secondary ions and the setup was not optimized to achieve high mass resolution. In fact, due to the delicate dual-polarity extraction, the mass resolution of the spectrometers is severely limited. Spectra acquired from an arginine sample using a 28 MeV ^{197}Au primary ion beam exhibiting a mass resolution m/Δm of only 10–20. Example spectra are shown in Fig. 3. The mass resolution is mainly restricted by the extraction field which has to be close to zero at the sample surface to allow the simultaneous escape of positive and negative ions towards the spectrometer arms. The initial energy distribution of the emitted ions therefore has a large influence on the total flight time of the ions.

However mass resolution is already sufficient to resolve the peaks or peak groups of monomer secondary ions and small molecular secondary ions from simple compounds. Combined with the unique event correlation possibilities of the setup, this allows new insights into the emission of secondary ions from primary ion impacts.

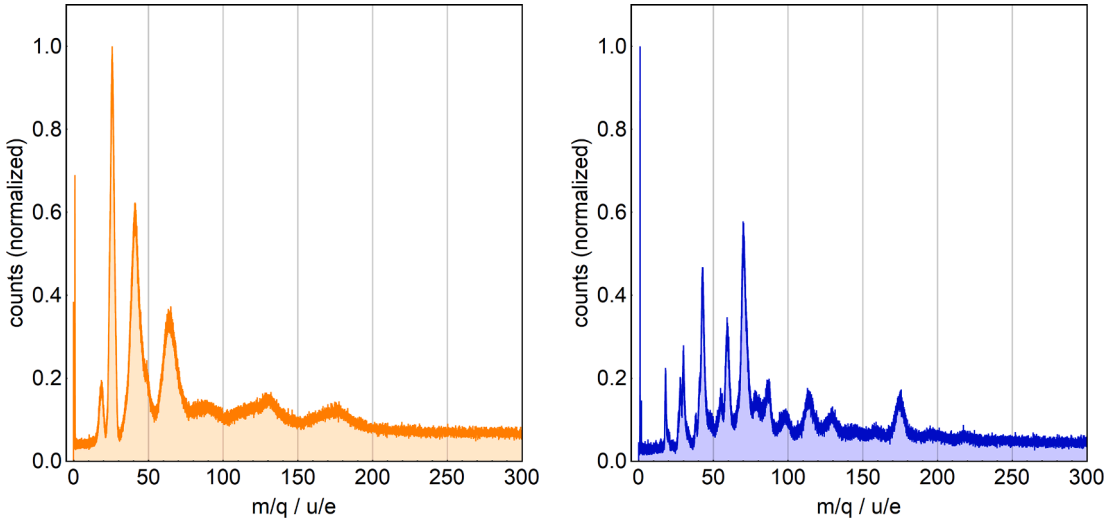

Fig. 3. Negative (left) and positive (right) secondary ion mass spectra of 28 MeV ^{197}Au on Arginine. These two spectra were acquired with a slightly modified tuning of the ToF spectrometer, resulting in lower mass resolution in the negative ion mass spectrum (left).

3. Measurements and discussion

The versatility of the 6 MV Tandem accelerator facility enables the use of a wide range of primary ion beams of different energies. Of specific interest is the ability to use very heavy primary ion species including cluster ions. Thus, studies of cluster effects in the emission yield of secondary ions become possible. Previous studies with positive secondary ions have observed a significant influence on both the secondary ion yield of molecular ions and their fragmentation [14], indicating a change in the desorption mechanism for secondary ions. This change can be characterized in more detail by measuring both polarities of secondary ions as well as secondary electrons, especially if all particles originating from a single impact are observed.

To study these effects, a set of measurements with small C_n cluster primary ions was performed. As cluster ions consisting of light individual constituents (with an atomic number of Z = 6), at an energy of 7 MeV these exhibit large ratios of electronic to nuclear stopping (between 200:1 and 800:1) at the sample surface. Secondary ions are therefore primarily desorbed through the mechanism of electronic sputtering. Additionally, it has been observed in previous studies [14] that yield enhancing and fragmentation reducing cluster effects are strongest for n < 5 and exhibit a saturation for larger primary cluster sizes. Arginine ($C_6H_{14}N_4O_2$, m = 174u) deposited onto cleaned Si-wafers by spin-coating was used as a sample material. Positive and negative secondary mass spectra acquired using 7 MeV C_6 cluster primary ions are shown in Fig. 4. The typical arginine fragment peaks [15] are observed in the positive spectrum with the most significant ones at masses m = 30u ($CH_2NH_2^+$), m = 43u ($CH_3N_2^+$), m = 70u ($C_4H_8N^+$). In the negative spectrum the most distinct fragment peaks appear at masses m = 26u, 41u, 66u. In both spectra the molecular arginine mass peak can be observed – represented by the positive hydrogenated $(M + 1)^+$ ion at mass m = 175u and the negative $(M-1)^-$ ion at mass m = 173u respectively.

3.1. Multiplicity of multi-stop events

During offline analysis, the detector events recorded in list-file mode were analysed: An event in the secondary electron detector channel is considered a start signal, if it is separated by at least the coincidence time (20 μs) from the preceding event. Each start signal is then correlated with stop signals from both ToF stop detector channels falling within the following coincidence time window of 20 μs. By correlating events within a single stop detector channel, the effects of the primary cluster size on the simultaneous emission of several secondary ions of one polarity from a single primary ion impact can be investigated. The distribution of multi-stop events, i.e. start signals that are correlated with more than one stop event in the corresponding ToF detector, is plotted in Fig. 5: The relative frequency of multi-stop events is shown as a function of the multiplicity (i.e. the number of stops signals observed per start signal) for spectra acquired with several primary monomer and cluster ion beams.

For all primary cluster sizes, negative secondary ions show a faster decrease of their multi-stop frequency with increasing multiplicity than positive ions (indicated by the steeper distribution curve for negative ions). However, the impact of a larger primary cluster ion results in a higher fraction of multiple secondary ion detections per primary ion: The fraction of impacts for which only a single secondary ion is detected is roughly halved for larger C_6 primary ions when comparing to C_1 elementary primary ions. Consequently, the frequency of multi-stop events is increasing by several orders of magnitude and their distribution shifts more and more towards higher multiplicities when increasing the primary cluster size. The multi-stop distribution measured with elementary C_1 primary ions shows a roughly exponential decrease with increasing multiplicity (straight line in linear-logarithmic plots), while the multiplicity distribution shifts towards a poisson-like dependency with increasing primary cluster ion size.

In conclusion it is apparent that larger primary cluster ions enhance the emission of multiple secondary ions from a single impact. The magnitude of this effect seems to depend on the secondary ion polarity. Generally, the multiplicity observed for negative secondary ions is lower than for positive secondary ions. Apart from an asymmetric tuning of the extraction (which is however rather biased in favour of negative ions) this could be explained by an excitation of a large percentage of the secondary ions. The negative ions can then decay into neutral particles, while positive ions do not have such a decay pathway.

3.2. Ratio of corresponding positive/negative ion yields

In a second analysis, the ratio of corresponding negative and positive secondary ion pairs was investigated. Two peak pairs were selected: The first at mass m = 43u for the positive ion and at mass m = 41u for the negative ion. These peaks correspond to the arginine fragments C_2H_3N and CH_3N_2, respectively. Due to the limited mass resolution, they cannot be separated from their neighbouring fragments CH_2N_2 and CH_4N_2. As the second peak pair, the full molecular arginine peaks corresponding to $(M + H)^+$ at mass m = 175u (positive) and $(M-H)^-$ at m = 173u (negative) were used.

For each of the selected mass peaks, ion yields were determined by

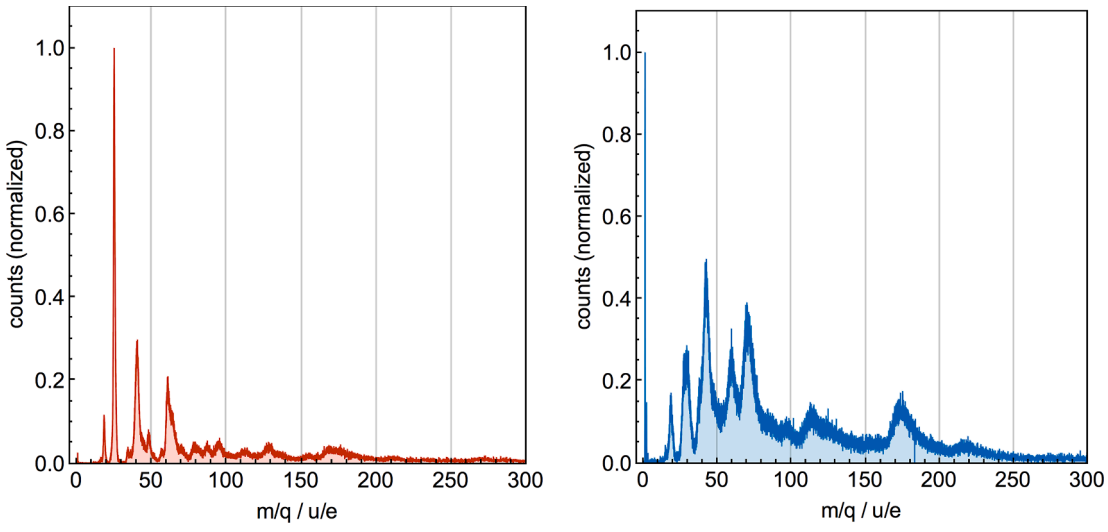

Fig. 4. Negative (left) and positive (right) spectra from impact of 7 MeV C_6 on arginine.

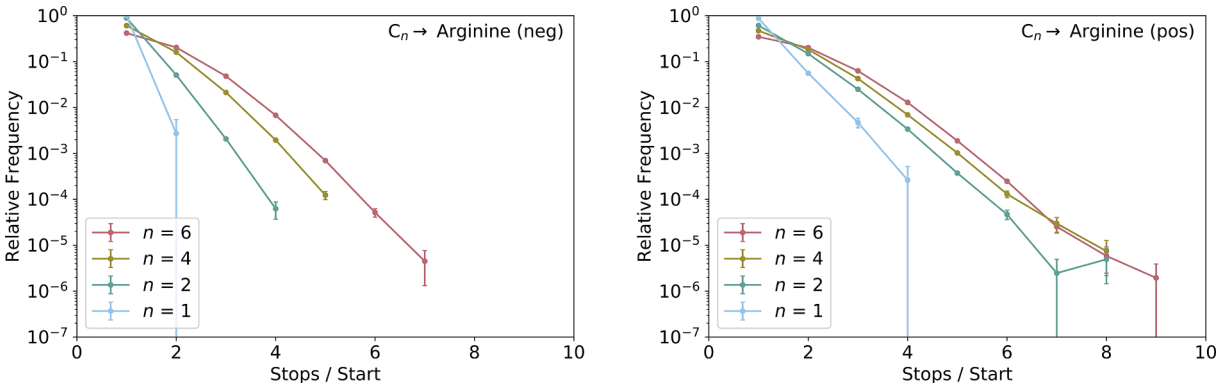

Fig. 5. Relative frequency of negative (left) and positive (right) multi-stop events recorded from arginine sample with 7 MeV C_n primary ion beams.

fitting individual mass peaks automatically with an exponentially modified gaussian peak function on top of a constant background. For each fit a number of fit parameters and the coefficient of determination R^2 were monitored and the resulting peak fits were inspected visually. From the peak fit the number of counts was computed by integration (while subtracting the constant background originating from random coincidences between the start and stop detectors) between pre-defined integration boundaries. Finally, the resulting yields were computed by normalization of the counts in the respective mass peak to the number of incident primary ions during the acquisition time of the spectrum. This number was determined from the measurement time and the average of two measurements of the primary ion count rate taken before and after each MeV-SIMS spectra acquisition with the transmission GID detector. The applied procedure is described in more detail in [14].

In Fig. 6 ion yields are plotted as a function of the primary C_n cluster ion size. For comparison the ratio between the respective positive and negative ion yields of the selected peak pair is shown. Despite the different secondary ions selected (fragment vs. full-mass molecule), the yield ratios of both ion pairs exhibit similar features. When bombarding the samples with monoatomic C primary ions, yields of the positive secondary ion are consistently higher than those of the corresponding negative secondary ion. By using primary C_n cluster ions, negative secondary ion yields increase with increasing cluster size n, such that the ratio of corresponding positive and negative secondary ion yields approaches values close to parity. The fact that this effect occurs across different secondary ion species suggests a drastic change in the actual underlying ionization process of the desorbed Arginine molecules and their fragments. While spatially isolated secondary emission events take place at low energy deposition densities more and more correlated multi-emission processes may be expected at the enormously enhanced energy and ionization densities induced by the impact of high energy cluster ions. Therefore, a possible explanation would be the formation of a plasma-like state at the primary ion impact point similar to the one induced by laser ablation of the sample material.

4. Conclusions and outlook

In summary, the existing CHIMP setup at ETH Zurich was upgraded to a new simultaneous dual polarity MeV-SIMS instrument. The new instrument demonstrates the feasibility of independent detection of secondary electrons as well as negative and positive secondary ions emitted from the sample after a single primary ion impact. The possibility to correlate the signals from all three secondary particle detectors with each other makes the setup a unique platform to study the underlying desorption and ionization processes in MeV-SIMS.

The capability for offline event correlation analysis was utilized for a first study with small primary C_n cluster ions resulting in the following observations: From a single monoatomic projectile impact on arginine negative secondary ions are emitted with lower multiplicity than positive ions. The use of larger primary cluster ions increases the emission multiplicity for both positive and negative secondary ions significantly. When simultaneously acquired positive and negative mass spectra are directly compared, the size of the impacting primary cluster ions influences the ratio of corresponding positive / negative secondary ion pairs. While positive ions are predominantly emitted from monoatomic primary ion impacts, the ratio shifts towards parity with increasing

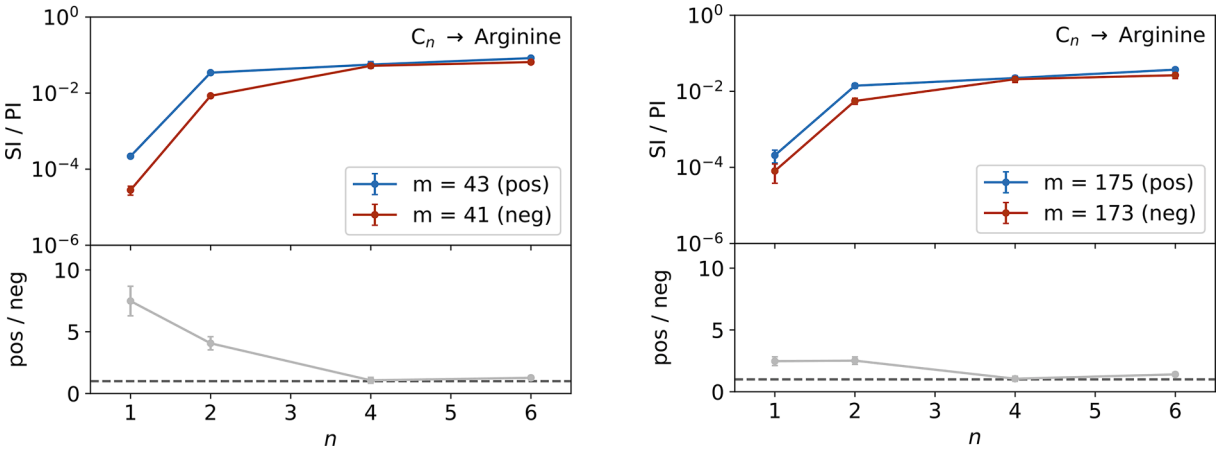

Fig. 6. Secondary ion yields of corresponding positive and negative ions as a function of primary C_n cluster size (upper panels) and their ratio (lower panels). The data for the fragment ion pair at masses m = 43u (positive) / m = 41u (negative) and the full mass molecular ion pair at masses m = 175u (positive) / m = 173u (negative) are shown in (a) and (b) respectively.

primary ion cluster size. This behaviour is exhibited by fragment as well as full mass molecular secondary ions. It is observed in addition to other cluster effects leading to yield enhancement and fragmentation reduction [14]. Therefore this yield ratio effect suggests a change of the secondary ion ionization process after the impact of a cluster ion.

The new setup was not designed to achieve high mass resolution and is thus limited by the delicate extraction field arrangement required for a dual polarity mass spectrometer. However, these first measurements clearly demonstrate its value to explore the underlying processes and contribute to an improved understanding of the emission of secondary ions in MeV-SIMS. While longer flight tubes would not overcome the limitations due to the extraction field geometry, the ion mirror of a reflectron mass spectrometer could reduce the kinetic energy spread of the ions. In any case, by switching operation to single-polarity mode and installation of a state of the art orthogonal-extraction mass spectrometer, applied research and imaging with significantly higher mass resolution should be possible.

CRediT authorship contribution statement

Klaus-Ulrich Miltenberger: Conceptualization, Methodology, Measurements and data analysis, Writing - original draft and review & editing. **Max Döbeli:** Conceptualization, Methodology, Analysis, Writing - review & editing, Supervision, Funding acquisition. **Christof Vockenhuber:** Conceptualization, Analysis, Writing - review & editing. **Hans-Arno Synal:** Conceptualization, Analysis, Writing - review & editing, Supervision, Funding acquisition.

Declaration of Competing Interest

The authors declare that they have no known competing financial interests or personal relationships that could have appeared to influence the work reported in this paper.

Acknowledgements

This work was supported by the Swiss National Science Foundation under contract No. 175653. The Laboratory of Ion Beam Physics is partially funded by its consortium partners PSI, EAWAG and EMPA.

Furthermore, we would like to thank the group of Prof. J. Matsuo at Kyoto University for the supply of arginine samples.

References

[1] B.N. Jones, J. Matsuo, Y. Nakata, H. Yamada, J. Watts, S. Hinder, V. Palitsin, R. Webb, Comparison of MeV monomer ion and keV cluster ToF-SIMS, Surf. Interface Anal. 43 (1-2) (2011) 249–252, https://doi.org/10.1002/sia.3520.

[2] Y. Nakata, Y. Honda, S. Ninomiya, T. Seki, T. Aoki, J. Matsuo, Matrix-free high-resolution imaging mass spectrometry with high-energy ion projectiles, J. Mass Spectrom. 44 (1) (2009) 128–136, https://doi.org/10.1002/jms.v44:110.1002/jms.1482.

[3] K. Wien, Fast heavy ion induced desorption, Radiat Eff. Defects Solids 109 (1-4) (1989) 137–167, https://doi.org/10.1080/10420158908220529.

[4] D.D.N.B. Daya, P. Demirev, J. Eriksson, A. Hallén, P. Håkansson, R.E. Johnson, J. Kopniczky, R.M. Papaléo, C.T. Reimann, J. Rottler, B.U.R. Sundqvist, Interaction of MeV atomic ions with molecular solids: Ion track structure and sputtering phenomena, Radiat. Meas. 28 (1-6) (1997) 101–110, https://doi.org/10.1016/S1350-4487(97)00048-6.

[5] F. Meinerzhagen, L. Breuer, H. Bukowska, M. Bender, D. Severin, M. Herder, H. Lebius, M. Schleberger, A. Wucher, A new setup for the investigation of swift heavy ion induced particle emission and surface modifications, Rev. Sci. Instrum. 87 (1) (2016) 013903, https://doi.org/10.1063/1.4939899.

[6] L. Breuer, P. Ernst, M. Herder, F. Meinerzhagen, M. Bender, D. Severin, A. Wucher, Secondary ion formation during electronic and nuclear sputtering of germanium, Nucl. Instrum. Methods Phys. Res., Sect. B 424 (2018) 1–9, https://doi.org/10.1016/j.nimb.2018.03.019.

[7] S.-T. Tsai, C.W. Chen, L.C.L. Huang, M.-C. Huang, C.-H. Chen, Y.-S. Wang, Simultaneous mass analysis of positive and negative ions using a dual-polarity time-of-flight mass spectrometer, Anal. Chem. 78 (22) (2006) 7729–7734, https://doi.org/10.1021/ac061213v.

[8] R.J. Chater, A.J. Smith, G. Cooke, Simultaneous detection of positive and negative secondary ions, J. Vacuum Sci. Tech. B, Nanotech. Microelectronics: Materials, Processing, Measurement, and Phenomena. 34 (3) (2016) 03H122, https://doi.org/10.1116/1.4943531.

[9] M. Schulte-Borchers, M. Döbeli, A.M. Müller, M. George, H.-A. Synal, Time-of-flight MeV-SIMS with beam induced secondary electron trigger, Nuclear Instruments and Methods in Physics Research Section B: Beam Interactions with Materials and Atoms. 380 (2016) 94–98, https://doi.org/10.1016/j.nimb.2016.05.011.

[10] K.-U. Miltenberger, M. Schulte-Borchers, M. Döbeli, A.M. Müller, M. George, H.-A. Synal, MeV-SIMS capillary microprobe for molecular imaging, Nucl. Instrum. Methods Phys. Res., Sect. B 412 (2017) 185–189, https://doi.org/10.1016/j.nimb.2017.09.024.

[11] M. Christl, C. Vockenhuber, P.W. Kubik, L. Wacker, J. Lachner, V. Alfimov, H.-A. Synal, The ETH Zurich AMS facilities: Performance parameters and reference materials, Nucl. Instrum. Methods Phys. Res., Sect. B 294 (2013) 29–38, https://doi.org/10.1016/j.nimb.2012.03.004.

[12] M.J. Simon, M. Döbeli, A.M. Müller, H.-A. Synal, In-air STIM with a capillary microprobe, Nucl. Instrum. Methods Phys. Res., Sect. B 273 (2012) 237–240, https://doi.org/10.1016/j.nimb.2011.07.084.

[13] A.M. Müller, M. Döbeli, M. Seiler, H.-A. Synal, A simple Bragg detector design for AMS and IBA applications, Nucl. Instrum. Methods Phys. Res., Sect. B 356–357 (2015) 81–87, https://doi.org/10.1016/j.nimb.2015.04.056.

[14] K.-U. Miltenberger, Secondary ion emission in MeV-SIMS, ETH Zurich (2020), https://doi.org/10.3929/ethz-b-000477725.

[15] B.T. Chait, W.C. Agosta, F.H. Field, Fission fragment ionization (252Cf) mass spectrometry. Positive and negative spectra and decomposition mechanisms for seven compounds, Int. J. Mass Spectrom. Ion Phys. 39 (3) (1981) 339–366, https://doi.org/10.1016/0020-7381(81)87007-6.